Michigan State University

National Superconducting Cyclotron Laboratory

BLAST OF LIGHT FRAGMENTS FROM CENTRAL HEAVY-ION COLLISIONS

PAWEL DANIELEWICZ and QIUBAO PAN

MSUCL-848

JUNE 1992

MSUCL-848

Blast of light fragments from central heavy-ion collisions

Paweł Danielewicz and Qiubao Pan
National Superconducting Cyclotron Laboratory,
and Department of Physics and Astronomy,
Michigan State University, East Lansing, Michigan 48824, USA

Abstract: The effects of collective expansion on light-fragment emission from central heavy-ion collisions are studied by carrying out calculations in a transport model with dynamic production of $A \leq 3$ fragments. Beam energies of few hundred MeV/nucleon are considered. In the simulations the formation of a region of dense excited nuclear matter is observed, which expands in transverse directions. The expansion is reflected in the angular distributions and in the mean transverse energies of emitted fragments. At the late stage of expansion the characteristic features of local thermodynamic equilibrium are identified. Different particles share nearly the same collective energy per nucleon, and nearly the same thermal energy. The calculated mean transverse energies of the fragments reflect the collective energy whose magnitude varies with impact parameter. However, the fragment energies only partially agree with available data. The calculated spectra exhibit different slopes at angles around c.m. 90" in central reactions.

PACS Numbers: 25.75.+r, 24.10.-i

I. INTRODUCTION

In the early hydrodynamic models of central heavy-ion collisions,[1] a region with dense excited matter was assumed to be formed in the center between colliding nuclei. The region primarily expanded in the directions perpendicular to the beam axis. Traces of a collective expansion, or blast wave, were searched for in the measured single-particle spectra from collisions, e.g., by comparing the inclusive pion and proton spectra.[2] The analyses of the 4π data[3] demonstrated unambiguously the existence of another form of collective motion, the deflection of fragments moving forward and backward in the system c.m in the semicentral collisions. Further, at midrapidity a preference was found for the fragments to be emitted out of the reaction plane at high beam energies,[4,5] and in the reaction plane at the low energies.[6] Observations that were not fully understood, but were likely related to the collective behavior of matter, included: the c.m. polar-angle 90° enhancement of proton emission in the central La+La reactions[7] at 246 MeV/nucleon, and the high values of ^{4}He and ^{3}He energies at c.m. 90° when compared to p, d, and t energies in Nb+Nb and Au+Au reactions[8] at 250 MeV/nucleon. The 90° enhancement of proton emission, possibly indicating sideward expansion, could not be produced in QMD calculations for impact parameters corresponding to the experiment. Recently, in the ^{36}Ar+Ag/Br reaction[9] at about 65 MeV/nucleon, the average c.m. fragment energy was observed to rise with the fragment charge in central events. The effect appeared to be absent in the ^{16}O+Ag/Br reaction[9] at about 210 MeV/nucleon. The description of the lower-energy data in the fragmentation model improved when the presence of a collective radial flow was assumed.

In this paper we study the effects of a collective expansion on the light fragment emission from central heavy-ion collisions, by carrying out calculations in a transport model with dynamic production of $A \leq 3$ fragments. We consider beam energies of few hundred MeV/nucleon. In the simulations we observe the formation of a region with dense excited matter that expands in transverse directions. This expansion is reflected in the angular distributions and in the transverse energies of emitted fragments. In the late stages of collisions, characteristic features of local thermodynamic equilibrium may be identified. Different particles share nearly the same collective energy per nucleon, and nearly the same thermal energy. The mean transverse energies of the fragments reflect the collective energy whose magnitude varies with impact parameter. However, the calculated fragment energies only partially agree with available data. The calculated spectra of the various fragments exhibit different slopes at angles around c.m. 90° in central reactions. Relevant details of our model are discussed in Sec. II. Calculations of heavy-ion collisions are presented in Sec. III. We conclude with a discussion of the results of calculations and measurements in Sec. IV.

II. TRANSPORT MODEL WITH COMPOSITE PRODUCTION

The transport model with dynamic deuteron production was introduced in Ref. 10. Here we extend that model to the production of A = 3 fragments.

The formation or breakup of a composite particle requires an external agent that acts differently on the different constituents. The individual nucleons may serve as such agents. The average nuclear potential was shown[11], on the other hand, to play no significant role in these processes at higher energies, being too weak and varying too slowly in space. In Ref. 10 the coupled transport equations for nucleons and deuterons, valid in the limit of slow spatial and temporal changes in the system, were derived from the Green's function equations of motion. We extend the set by adding the transport equations for A = 3 composites and coupling terms, exploiting our past experience,[10,12] without going through a full derivation (see also Refs. 13 and 14).

The equations take the form

$$\frac{\partial f_x}{\partial t} + \frac{\partial E_x}{\partial \mathbf{p}}\cdot\frac{\partial f_x}{\partial \mathbf{r}} - \frac{\partial E_x}{\partial \mathbf{r}}\cdot\frac{\partial f_x}{\partial \mathbf{p}} = \mathcal{K}_x^{<}(1 \mp f_x) - \mathcal{K}_x^{>} f_x \; . \qquad (2.1)$$

Here f_x is the Wigner function, and $\mathcal{K}_x^{<}$ and $\mathcal{K}_x^{>}$ are, respectively, the production and absorption rates of the particle x. The lower bosonic sign in (2.1) is for deuterons and the upper sign is for the odd-A particles. The term in the helion production rate accounting for the formation of helions in the interaction of four nucleons may be written as

$$\mathcal{K}_h^{<}(\mathbf{p}) = 8\,\frac{m_h}{E_h(\mathbf{p})}\int\frac{d\mathbf{p}_1}{(2\pi)^3}\,\frac{m_N}{E_N(\mathbf{p}_1)}\int\frac{d\mathbf{p}'}{(2\pi)^3}\,\frac{m_N}{E_N(\mathbf{p}')}\int\frac{d\mathbf{p}_1'}{(2\pi)^3}\,\frac{m_N}{E_N(\mathbf{p}_1')}\int\frac{d\mathbf{p}_2'}{(2\pi)^3}$$

$$\times \; \frac{m_N}{E_N(\mathbf{p}_2')} \int \frac{d\mathbf{p}_3'}{(2\pi)^3} \frac{m_N}{E_N(\mathbf{p}_3')} \, 2\pi\delta(E_h(\mathbf{p}) + E_N(\mathbf{p}_1) - E_N(\mathbf{p}')$$

$$- E_N(\mathbf{p}_1') - E_N(\mathbf{p}_2') - E_N(\mathbf{p}_3'))(2\pi)^3\delta(\mathbf{p} + \mathbf{p}_1 - \mathbf{p}' - \mathbf{p}_1'$$

$$- \mathbf{p}_2' - \mathbf{p}_3')\Big\{\tfrac{1}{6}\overline{|\mathcal{M}_{3pn\to ph}|^2} f_p(\mathbf{p}')(1 - f_p(\mathbf{p}_1)) + \tfrac{1}{4}\overline{|\mathcal{M}_{ppnn\to nh}|^2}$$

$$\times f_n(\mathbf{p}')(1 - f_n(\mathbf{p}_1))\Big\} f_p(\mathbf{p}_1') f_p(\mathbf{p}_2') f_p(\mathbf{p}_3') + \ldots \; . \qquad (2.2)$$

The factors $\overline{|\mathcal{M}|^2}$ stand for the matrix elements squared summed over the final and averaged over the initial spin directions. The dots indicate other terms in the production rate. A term in the helion absorption rate accounting for the helion breakup into nucleons has an analogous form to the term for the formation (2.2), with statistical factors for the initial and final states interchanged. The matrix elements for the processes are related by

$$\overline{|\mathcal{M}_{4N\to Nh}|^2} = \frac{1}{2}\overline{|\mathcal{M}_{Nh\to 4N}|^2} \; , \qquad (2.3)$$

and the matrix element for the breakup is related to the breakup cross section by

$$d\sigma_{Nh\to 4N} = \frac{1}{v_1} \frac{m_N}{E_N(\mathbf{p}_1)} \overline{|\mathcal{M}_{4N\to Nh}|^2} \, 2\pi\delta(m_h + E_N(\mathbf{p}_1) - E_N(\mathbf{p}_1') - E_N(\mathbf{p}_2')$$

$$- E_N(\mathbf{p}_3') - E_N(\mathbf{p}_4'))(2\pi)^3\delta(\mathbf{p}_1 - \mathbf{p}_1' - \mathbf{p}_2' - \mathbf{p}_3' - \mathbf{p}_4') \frac{m_N}{E_N(\mathbf{p}_1')}$$

$$\times \frac{d\mathbf{p}_1'}{(2\pi)^3} \frac{m_N}{E_N(\mathbf{p}_2')} \frac{d\mathbf{p}_2'}{(2\pi)^3} \frac{m_N}{E_N(\mathbf{p}_3')} \frac{d\mathbf{p}_3'}{(2\pi)^3} \frac{m_N}{E_N(\mathbf{p}_4')} \frac{d\mathbf{p}_4'}{(2\pi)^3} \; , \qquad (2.4)$$

where we assume that helion is at rest in the initial state. The δ-functions of energy and momentum conservation may be our set of equations yields the required law of mass action.

We generally use the following parametrization for single-particle energies in the system c.m.,

$$E_x = (p^2 + m_x^2)^{1/2} + q\Phi ,$$

$$m_x = m_{x0} + AU + t_3U_1 . \tag{2.6}$$

Here q is charge, Φ - Coulomb potential, m_{x0} - mass in free space, and t_3 is isospin. The functional dependence of the potentials U and U_I on the scalar densities is chosen as in nonrelativistic calculations,

$$U = -a(\rho_s/\rho_s^0) + b(\rho_s/\rho_s^0)^\sigma , \tag{2.7}$$

$$U_1 = c(\rho_s^T/\rho_s^0) , \tag{2.8}$$

where

$$\rho_s = \sum_x A\ \rho_s^x , \quad \rho_s^T = \sum_x t_3\rho_s^x , \tag{2.9}$$

$$\rho_s^x = g_x \int \frac{d\mathbf{p}}{(2\pi)^3} \frac{m_{x0}}{E_x} f_x , \tag{2.10}$$

and g is spin degeneracy. The case of a = 348 MeV, b = 298 MeV, and σ = 7/6 in (2.7), corresponds to the soft equation of state, and a = 119 MeV, b = 68.5 MeV, and σ = 2, to the stiff equation; $\rho_s^0 \simeq \rho^0 \simeq 0.145\ \mathrm{fm}^{-3}$ and c = 92 MeV. Principally, the systems considered in this paper are nonrelativistic in their center of mass. Unless otherwise stated, the results of our calculations are for the first set of parameters. The Coulomb potential is calculated by solving the Poisson equation as outlined in Ref. 17. Other details can be found in Ref. 10.

III. HEAVY-ION COLLISIONS

We report here the calculations of central collisions of heavy symmetric systems, for beam energies of few hundred MeV/nucleon. In this energy range, we can compare our results with the data which seem to display interesting effects of the expansion in collisions.

A. Collision dynamics and angular distributions

Figure 1 shows the evolution of the density of particles, projected onto the reaction plane, in the Au + Au collisions at 250 MeV/nucleon. At the early stages of the reaction, the matter in the central region between nuclei gets compressed and heated. The baryon density along and perpendicular to the beam axis at an early time instant is shown in Fig. 2, for $b = 0$. A shock-like discontinuity separating the excited and cold matter, perpendicular to the beam axis, may be identified in the figure. Maximum densities reached in the collisions of heavy nuclei are displayed in Fig. 3 as a function of the beam energy. The solid line shows the density expected for our equation of state if all available energy per nucleon were used up in thermalization and compression. The Coulomb repulsion reduces the compression for a given beam energy, but even when this repulsion is switched off, a density from the naive expectation is not reached. That is because the thermalization is not complete early in the reactions, even for heavy nuclei (see also Refs. 19 and 20).

After compression, the matter expands into the vacuum. At a later stage of the process, the light composites are produced, see Fig. 4. In our model composites which are broken actually outnumber considerably those which avoid breakup and reach the vacuum. For b = 0 the system preferentially expands in the transverse direction, cf. Figs. 1 and 2. In Fig. 2 it can be seen that matter expands in the direction perpendicular to the beam axis, while along the beam axis a compression still takes place. In the bottom panel of Fig. 4 we show the growth, with time, of the collective transverse energy

$$E_\perp^{coll} = \int d\mathbf{r} d\mathbf{p}\ f\ \tfrac{1}{2} m (v_\perp^{coll})^2 \Big/ \int d\mathbf{r} d\mathbf{p}\ f\ , \qquad (3.1)$$

per nucleon, of the participant nucleons and of the light composites. The collective velocity $\mathbf{v}_\perp^{coll}$ in (3.1) is calculated locally, using only those particles from the surroundings that have participated in collisions. We cease to update the collective velocity for a particle, once the density of the surrounding matter drops below $\rho^0/8$, as the concept of a collective velocity can make sense only when interactions are frequent.

With increasing impact parameter, the expanding and approximately ellipsoidal region of matter at the late stages of a collision is no longer perpendicular, but at some angle to the beam axis, see Fig. 1 (compare also the results of hydrodynamic calculations of Ref. 21). Figure 5 shows the final polar-angle distributions for central impact parameters in two reactions: La + La at bombarding energy of 246 MeV/nucleon, and Au + Au at 250 MeV/nucleon. Angular distributions of particles in these reactions peak at 90° for lowest impact parameters, and at 0°

for b $\geq$ 3 fm.

Experimentally,[7] the cross sections for emission of protons with c.m. kinetic energies above 90 MeV, in the very central La + La collisions at 246 MeV/nucleon, were found to be (1.5 - 2) times higher at c.m. 90° than at 40°. The QMD calculations gave basically equal cross sections under the experimental conditions for the two angles. The measured events correspond to impact parameters between 0 and 3 fm, and a median impact parameter of about 2 fm. At b = 2 fm, we do obtain more protons emitted per unit spherical angle at 90°, than at 40°, but the increase is only by a factor of 1.2. A restriction to the protons with c.m. energy above 90 MeV does not raise the ratio of proton numbers for the two polar angles. The discrepancy between the data and calculations could mean that there is not enough stopping in the model. In any case, our calculations appear to rule out the explanation of the observed effect as caused by an 'eating up' of protons by the clusters forming in a more forward region. In central collisions we get a stronger 90° peaking for the composites than for nucleons. Experimental investigation of the effect for composite particles would certainly be desirable.

As the preference for the polar-angle 90° emission disappears, with the increase of impact parameter and the rotation of emission pattern about an axis perpendicular to the reaction plane, the remainder of the effect for low b becomes the squeeze out.[5] This observed effect is a preference for the emission of particles in the azimuthal angle out of the reaction plane, at midrapidity. Experimentally, the reaction plane direction may be determined using the opposite sideward deflection of particles moving forward and backward in the system c.m. Measured[5] and calculated azimuthal distributions about the beam axis at midrapidity, in the semi-central Au + Au collisions at 400 MeV/nucleon, are shown in Fig. 6. These results appear quite consistent. In the simulation we find that distributions for composites are a bit more asymmetric than for protons. The azimuthal asymmetries can be amplified, see Fig. 7, by rotating[5] the coordinate axes in the reaction plane, making the third axis coincide with the major axis of the sphericity tensor defined as

$$S^{ij} = \sum_{\nu=1}^{M} p_\nu^i p_\nu^j / 2m_\nu \,, \tag{3.2}$$

where the summation is over particles from a collision. For a heavy system the azimuthal angle φ' about the major axis of this tensor becomes identical to the polar angle θ when the impact parameter tends to zero. Just then the emission in the angle φ about the beam axis becomes trivially isotropic.

B. Mean transverse energies

We now turn to the measured and calculated values of transverse energies of emitted light fragments and their relation to the collision dynamics. The energies of fragments emitted into c.m. 90° in three symmetric systems were measured in Ref. 8 at beam energies between 150 and 800 MeV/nucleon. At all beam energies the mean transverse energies were observed to rise with increasing charged particle multiplicity, with maximum proton energies significantly exceeding average c.m. energies per nucleon. Most strikingly, in the Nb + Nb and Au + Au collisions at 250 MeV/nucleon, the helium isotopes were found to be emitted with higher transverse energies than the hydrogen isotopes, with energy differences rising quite dramatically with increasing multiplicity in the collisions (see the left panels in Fig. 8). In a system approaching thermal equilibrium, one generally expects the average kinetic energies of different particles to be equal! In Fig. 8, besides the data, we show as a function of impact parameter the results of our model calculation in a direct form (right panels), and with the final state subjected to a numeric procedure[22] simulating detector inefficiencies (center panels). Note that the impact parameters *decrease* on the average when going from left to right in the panels with data. We consider the results of measurements and calculations of considerable importance and proceed to discuss them in detail.

We start with our basic findings. A significant part of proton transverse energy in the collisions has its origin in the composite formation that frees up kinetic energy. This is demonstrated for Nb + Nb collisions in the right panel of Fig. 8, where we show proton energies when composite formation is switched off in the calculation. In general, the rise of proton transverse energy with multiplicity could be due exclusively to an increased number of composites relative to nucleons at low impact parameters. However, it can be seen in Fig. 8 that the energy rises even when the composite formation is switched off. In the calculations we find that, due to Coulomb interactions, protons leave the collision region with higher energies than neutrons - by about 15 MeV at $b = 0$ in the case of Au + Au collision at $b = 0$, and by about 9 MeV in the case of Nb + Nb collision.

The calculated proton transverse energies are roughly consistent with the data, as are the ^{3}He energies. Under a closer examination, the proton energies for Nb + Nb collisions, and the ^{3}He energies for Au + Au collisions, are somewhat low. The calculation appears to reproduce the rise of average transverse energies in the most central collisions when going from the Nb + Nb to Au + Au system. The calculated deuteron energies are too high compared to the data, and even more so the triton energies. The procedure simulating detector inefficiencies lowers the energies of these particles, but not enough to bring about consistency. After the reasons for the high energies of composites in the simulations are comprehended, it may be expected that if the ^{4}He particles were included in the calculations, their energies would roughly agree with the Nb + Nb data, but disagree with the Au + Au data.

Generally, reasons for the rise of the mean transverse energy with the mass of a fragment might be varied. With the empirical scaling

$$f_X(\mathbf{p}) \propto [f_N(\mathbf{p}/A)]^A \, , \tag{3.3}$$

the rise of the energies could be produced by nonequilibrium features of the nucleon momentum distribution f_N, in particular by[23] a 'shoulder-arm' associated with the energy-momentum conservation in first scatterings. Our transport model should adhere to (3.3), if particle emission does not vary significantly with space and time. Nevertheless, a major role of nonequilibrium effects in the rise of energies with fragment mass can be ruled out in the collisions of interest for the following reason. The nonequilibrium effects are most important for high impact parameters, while the rise is most pronounced for low impact parameters. In central collisions the system is expected to be closest to equilibrium, and a collective flow, with *local* thermodynamic equilibrium, may be investigated as an explanation of the rise.

C. Blast interpretation of transverse energies

In an equilibrated system, expansion differently affects different mass fragments. Below we first derive, under certain assumptions, simple formulas for mean energies in a locally equilibrated system. We then use these formulas in interpreting the results of simulations. The differences in the energies of different mass fragments are linked to the differences in the collective energies proportional to the mass.

Local equilibrium distributions at low densities are, generally, of the form

$$f_X = \exp(-(u^\sigma p_\sigma - \mu_X)/T) \ , \tag{3.4}$$

where $u^\sigma = (\gamma, \gamma\mathbf{v})$, $\mathbf{v}$ is velocity field common for all species, μ is chemical potential, and T - temperature. We first consider particle transverse energies averaged over all angles, assuming that the system is approximately nonrelativistic in the center of mass, and μ and T are uniform. The transverse $E_\perp$ and longitudinal $E_{||}$ energies can be, in general, separated out from the particle kinetic energy E_{kin} according to

$$E_{kin} = \sqrt{m^2 + p^2} - m = \frac{p_\perp^2}{m + E} + \frac{p_{||}^2}{m + E} = E_\perp + E_{||} , \quad (3.5)$$

where $p_\perp$ and $p_{||}$ are, respectively, the transverse and longitudinal momentum components. Under our assumptions, the mean transverse energy becomes

$$\langle E_{\perp x}\rangle \simeq T + m_x\langle v_\perp^2\rangle/2 = T + E_{\perp x}^{coll} \simeq T + AE_{\perp N}^{coll} , \quad (3.6)$$

and it increases linearly with the mass number, with a coefficient given by the nucleon collective energy or collective energy per nucleon. The mean longitudinal energy becomes, at the same time,

$$\langle E_{||x}\rangle \simeq T/2 + m_x\langle v_{||}^2\rangle/2 = T/2 + E_{||x}^{coll} . \quad (3.7)$$

A simple result for the mean kinetic energy at 90° may be derived assuming that the distribution of transverse energies factorizes out in a Gaussian form,

$$\int d\mathbf{r}\ \rho(\mathbf{r})\ \delta(\mathbf{v} - \mathbf{v}(\mathbf{r})) \propto \exp(-v_\perp^2/\langle v_\perp^2\rangle) . \quad (3.8)$$

Then

$$\langle E_{\perp x}\rangle_{90^\circ} = \frac{3}{2}(T + E_{\perp x}^{coll}) \simeq \frac{3}{2}(T + AE_{\perp N}^{coll}) , \quad (3.9)$$

i.e. the mean energy at 90° increases linearly with the mass number, with a coefficient equal to 3/2 of the transverse collective energy per nucleon. When (3.8) is valid then, further, the mean transverse energy calculated at any fixed longitudinal momentum, e.g. $\langle E_{\perp x}\rangle_{p_{||}=0}$, is identical to the energy averaged over angles (3.6).

With all the assumptions that were adopted, the results obtained in (3.4)-(3.9) may be expected to be valid for the energies of particles emitted from a system, in an exact sense, only if all interactions stop instantaneously. Though the latter is not the case in our simulations, it will be seen that the relations apply quite well, at low impact parameters, to suitably-defined particle freeze-out energies. When considering the final particle energies one has to take into account the effects of Coulomb and nuclear potentials in the final state.

In the three panels in Fig. 9, we show as a function of impact parameter different energies in the simulations of Au + Au collisions at 250 MeV/nucleon. In the order from top to bottom these energies are: the final transverse energies averaged over angles of different fragments, the collective transverse energies from Eq. (3.1) for fragments with different mass, and the excitation energies at freeze-out

$$E^{*}_{\perp,||} = \langle E_{\perp,||}\rangle - E^{coll}_{\perp,||} \ . \tag{3.10}$$

The values of $\langle E_{\perp,||}\rangle$ in (3.10) are calculated at $\rho \simeq \rho^0/8$, and the collective longitudinal energy $E^{coll}_{||}$ is calculated in a similar manner as the transverse. For low b in the center panel it is seen that the collective transverse energy is, to first approximation, linear in the mass number (see also Fig. 4). For low b in the bottom panel of Fig. 9 it is observed that the transverse excitation energies are twice as large as the longitudinal excitation energies, and the energies are the same for fragments with different mass. These excitation energies are consistent with a local equilibrium with temperature $T \simeq 30$ MeV (cf. Eqs. (3.6) and (3.7)). For comparison, the temperature of the system in the fireball model, with no composite production, would be $T \simeq 34$ MeV.

Besides the values of final $\langle E_\perp \rangle$ in the top panel in Fig. 9, we show with crosses the values of $2\langle E_{\parallel p} \rangle$, i.e. twice the proton longitudinal energy averaged over angles. For lowest impact parameters we find $\langle E_{\perp p} \rangle > 2\langle E_{\parallel p} \rangle$. The crossover of $\langle E_{\perp p} \rangle$ and $2\langle E_{\parallel p} \rangle$ at $b \simeq 3$ fm is in qualitative agreement with the change of the emission pattern in the polar angle, Fig. 5. Overall, for low b the transverse energies in the top panel in Fig. 9 are about 2/3 of energies in the right panel for Au + Au collisions in Fig. 8, in conformance with (3.6) and (3.9). For low b the differences between the calculated triton and deuteron energies, in the top panel in Fig. 9 and in the right panels in Fig. 8, are nearly as large as the differences between the deuteron and proton energies, in conformance with Eqs. (3.6) and (3.9). The isotopic energy differences are not affected by the Coulomb field in the final state. At $b \simeq 0$ we get, for Au + Au,

$$\langle E_{\perp d} \rangle_{90^\circ} - \langle E_{\perp p} \rangle_{90^\circ} \simeq 24 \text{ MeV} , \tag{3.11}$$

and

$$\langle E_{\perp d} \rangle - \langle E_{\perp p} \rangle \simeq 18 \text{ MeV} , \tag{3.12}$$

of which the ratio is not quite 3/2 (cf. (3.6) and (3.9)), indicating a limited validity of (3.8).

An issue that requires explanation is why the differences in the *final* transverse energies, for hydrogen isotopes, are systematically lower than the differences in collective energies *at freeze-out* (see top and center panels in Fig. 9). For b ≃ 0 in the Au + Au collisions, we find

$$E_{\perp d}^{coll} - E_{\perp p}^{coll} \simeq 26 \text{ MeV} , \qquad (3.13)$$

to be compared with (3.12). The discrepancy is due to the nuclear mean-field which is still finite at the freeze-out density. The potential energy per nucleon corresponding to (2.7) at $\rho = \rho_0/8$ is -9.6 MeV. During the expansion, the kinetic transverse energy is reduced by more than 2/3 of this potential energy, when b ≃ 0. Upon switching off the nuclear potentials in the calculation, cf. Eq. (2.6), the differences in collective energies at the chosen freeze-out density, and the isotopic differences in the final angle-averaged transverse energies, become nearly identical.

The differences between mean helion and triton transverse energies in the simulation are generated by the Coulomb field in the final state. These differences nearly equal the differences between proton and neutron energies, and they disappear when Coulomb potential is switched off.

Attempting to resolve the discrepancies between data and calculations in the mass and charge dependencies of transverse energies, evident in Fig. 8, we have investigated the possible role of Coulomb field in the initial state. The Coulomb energy of a proton on the surface of a gold nucleus is about 16 MeV, and in a constrained static situation, e.g. with two gold nuclei touching, the Coulomb interactions could push out protons to the periphery of a system. In the collision, a redistribution of particles could, in general, lead to the different dynamics for protons and neutrons. However, at 250 MeV/nucleon the nuclei approach each other too fast for a significant polarization in the system to occur. We estimate that the relative displacement of protons and neutrons at the facing surfaces of the nuclei might be about 0.5 fm at the time of contact, due to the Coulomb repulsion of the other nucleus. In any case we have carried out a calculation separating the centers of nuclei by 35 fm in the initial state, finding no particular change in the transverse energies, as compared to the usual calculation with the nuclei initialized in the ground state with the surfaces nearly touching. At low energies the initial-state Coulomb-effects might be quite significant in the collisions of heavy nuclei, while they are generally ignored in the transport calculations.

We should mention that we have carried out calculations with a Pauli principle switched off for all particles, in order to see whether our results might not be affected by our treatment of the composites, cf. Sec. 2. We found the transverse-energy differences and the flow of the same order of magnitude as in standard calculations.

It is rather fortunate that the simulated nuclear systems appear to freeze-out at a constant temperature for low impact parameters. Changing temperatures and velocities, with space and time, could make an identification of the expansion of an equilibrated system much more difficult, see also Ref. 8.

D. Further predictions

We now present some further results of our model calculations. These include transverse energy spectra, the mean energy components in and out of the reaction plane, and the beam energy dependence of the blast. Finally, we address the sensitivity of the differences of mean transverse energies to the equation of state and the collision rates.

In Fig. 10 we show the calculated transverse energy spectra of particles emitted from the $b = 0$ Au + Au reaction at 250 MeV/nucleon, and from the Nb + Nb reaction at 400 MeV/nucleon. The proton spectrum from the latter reaction may be compared with the high-multiplicity selected data.[24] At higher fragment energies the calculated spectra are exponential in each of the reactions. The slopes are different for fragments with different mass numbers. With this the spectra violate the scaling relation (3.3) that would imply equal slopes for the fragments. At low energies the proton spectra exhibit a shoulder, while composite spectra definitely peak at finite kinetic energies. The Coulomb field in the final state contributes to these features. When the Coulomb potential is switched off, the proton shoulder disappears, while the peaks in composite spectra turn into shoulders. The latter indicates, in itself, that the velocity distribution is given by a more complicated function than (3.8).

Azimuthal distributions at midrapidity exhibit observable anisotropies associated with the reaction plane, as has been discussed in Subsection A. One may ask then whether the mean kinetic-energy components in and out of the reaction plane differ from one another, at midrapidity. We define the two components as $E_1 = p_1^2/(m + E)$ and $E_2 = p_2^2/(m + E)$, where p_1 and p_2 are transverse momentum components in and out of the reaction plane, respectively. The mean values calculated at midrapidity, $\langle E_1 \rangle_{p_{||}=0}$ and $\langle E_2 \rangle_{p_{||}=0}$, appear rather close. However, one can rotate the coordinate axes in the reaction plane as in Subsection A, making them coincide with the axes of a sphericity tensor (3.2). With momentum components along the minor and major axes of the tensor in the reaction plane p_1' and p_3', a distinctly different behavior is then obtained for the in and out of plane mean energies $\langle E_1' \rangle_{p_3'=0}$ and $\langle E_2 \rangle_{p_3'=0}$, see Fig. 11. Note that as $b \to 0$, the axis 1′ points in the beam direction. By the way of contrast between the two directions, Fig. 11 clearly demonstrates the collectivity of matter squeezed out of the reaction plane in our simulations.

We now briefly turn to the bombarding energy dependence of the collective expansion. The strength of the blast, as measured by the isotopic energy differences at 90°, increases rapidly with bombarding energy, for the beam energies up to about 300 MeV/nucleon, and then rather slowly, see Fig. 12. Relative to the beam energy the blast decreases in strength above 300 MeV/nucleon.

We have carried out only limited tests of the sensitivity of the mean-energy differences to the equation of state and collision rates, as the mere existence in nature of such differences attributable to collective expansion, cannot be claimed right now. In the very central Au + Au collisions at 250 MeV/nucleon, the change from a soft to stiff equation of state increases the differences in the mean fragment energies at 90° by about 3 MeV per unit mass difference. At the same time, the reduction of collision rates by a factor of 2 decreases the energy differences at 90° by about 8 MeV per unit mass difference.

IV. DISCUSSION

In the transport-model simulations of central symmetric collisions of heavy nuclei, at beam energies of few hundred MeV/nucleon, we observe a formation of the region with a dense excited nuclear matter that expands predominantly in the sideward directions. The expansion leads to a 90° peaking of particle distributions in the polar angle at lowest impact parameters, and to an out-of-the-reaction-plane peaking of distributions in the azimuthal angle at larger impact parameters. Compared to La + La data[7] at 246 MeV/nucleon, our calculation gives too weak 90° polar-angle peaking in central collisions. This could indicate too little stopping and not enough collectivity in the expansion of nuclear matter in our simulation. The calculated azimuthal distributions in the Au + Au collisions at 400 MeV/nucleon appear to agree, on the other hand, with data.[5]

Measurements[8] and calculations show some differences in the mean energies of various light fragments emitted into 90°, in the Nb + Nb and Au + Au reactions at 250 MeV/nucleon. These differences increase with a decreasing impact parameter. The measured energies of helium isotopes in the reactions are higher than the energies of hydrogen isotopes, by more than 40% at low impact parameters, and in the studied Au + Au reaction the measured energies of two helium isotopes are quite different. On the other hand, the measured energies of three hydrogen isotopes are rather close. In our calculations all different fragments with $A \leq 3$ have different mean energies at 90°.

The isotopic energy differences in our calculations are due to the collective expansion of the matter. The motion is organized by frequent collisions that locally equilibrate the system. Characteristic features of a collective expansion continue to be found in the calculations with some arbitrarily changed conditions. A natural explanation for the equal transverse energies of hydrogen isotopes observed in the experiment, would be a global equilibrium. However, in order to maintain such an equilibrium, the different parts of the system would need to communicate over tens of femtometers, during the rapid expansion! Except for the difference in Coulomb acceleration in the final state, the dynamics of the two $A = 3$ isobars are rather similar in the simulation. It is difficult to invent a mechanism that would generate as large transverse-energy difference between the two isobars as seen in the experiment.[8]

The subject of a collective expansion is of general interest. We hope that the phenomena observed in the simulations are sufficiently transparent, and the model itself involves sufficiently realistic elements, in order to motivate a reexamination of transverse energies of light fragments produced in the central heavy-ion collisions. Compared to the other presently done experimental analysis the determination of energies is rather straightforward. To the extent that our interpretation of energies could withstand the comparison with data, the transverse energy differences might be used for assessing the collective energy of sideward expansion in collisions.

ACKNOWLEDGEMENTS

We thank Walt Benenson, Roy Lacey, Romualdo de Souza, and Kim Sneppen for discussions. We also thank Gerd Welke for a critical reading of the manuscript. This work was supported by the National Science Foundation under Grant No. PHY-9017077.

REFERENCES

[1]W. Scheid, B. Müller, and W. Greiner, Phys. Rev. Lett. **32**, 741 (1974); M. I. Sobel, P. J. Siemens, J. P. Bondorf, and H. A. Bethe, Nucl. Phys. **A251**, 502 (1975).

[2]P. J. Siemens and J. O. Rasmussen, Phys. Rev. Lett. **42**, 880 (1975); H. Stöcker, A. A. Ogloblin, and W. Greiner, Z. Phys. A **303**, 253 (1981).

[3]H. Å. Gustafsson, H. H. Gutbrod, B. Kolb, H. Löhner, B. Ludewigt, A. M. Poskanzer, T. Renner, H. Riedesel, H. G. Ritter, A. Warwick, F. Weik, and H. Wieman, Phys. Rev. Lett. **52**, 1590 (1984); R. E. Renfordt, D. Schall, R. Bock, R. Brockmann, J. W. Harris, A. Sandoval, R. Stock, H. Ströbele, D. Bangert, W. Rauch, G. Odyniec, H. G. Pugh, and L. S. Schroeder, Phys. Rev. Lett. **53**, 763 (1984).

[4]P. Danielewicz, H. Ströbele, G. Odyniec, D. Bangert, R. Bock, R. Brockmann, J. W. Harris, H. G. Pugh, W. Rauch, R. E. Renfordt, A. Sandoval, D. Schall,L. S. Schroeder, and R. Stock, in *Proc. XV Workshop on Gross Properties of Nuclei and Nuclear Excitations*, Hirschegg, 1987, ed. H. Feldmeier, p. 91; Phys. Rev. C **38**, 120 (1988).

[5]H. H. Gutbrod, K. H. Kampert, B. Kolb, A. M. Poskanzer, H. G. Ritter, and H. R. Schmidt, Phys. Lett. B **216**, 267 (1989).

[6]W. K. Wilson, W. Benenson, D. A. Cebra, J. Clayton, S. Howden, J. Karn, T. Li, C. A. Ogilvie, A. Vander Molen, G. D. Westfall, J. S. Winfield, B. Young, and A. Nadasen, Phys. Rev. C **41**, R1881, (1990).

[7]G. Claesson, G. Krebs, J. Miller, G. Roche, L. S. Schroeder, W. Benenson, J. van der Plicht, J. S. Winfield, G. Landaud, J.-F. Gilot, C. Hartnack, and H. Stöcker, Phys. Lett. B **251**, 23 (1990).

[8]H. Å. Gustafsson, H. H. Gutbrod, K. H. Kampert, B. W. Kolb, A. M. Poskanzer, H. G. Ritter, and H. R. Schmidt, Mod. Phys. Lett. A **3**, 1323 (1988).

[9]H. W. Barz, J. P. Bondorf, R. Donangelo, R. Elmér, F. S. Hansen, B. Jakobsson, L. Karlsson, H. Nifenecker, H. Schulz, F. Schussler, K. Sneppen, and K. Söderström, Nucl. Phys. **A531**, 453 (1991).

[10]P. Danielewicz and G. F. Bertsch, Nucl. Phys. **A533**, 712 (1991).

[11]P. Danielewicz, in *Proc. Int. Workshop on Dynamical Fluctuations and Correlations in Nuclear Collisions*, Aussois, 1992, eds. M. Płoszajczak and E. Suraud.

[12]P. Danielewicz and P. Schuck, Phys. Lett. B **274**, 268 (1992).

[13]E. A. Remler, in *The Physics of Phase Space*, eds. Y. S. Kim and W. W. Zachary (Springer-Verlag, Berlin, 1986).

[14]G. Röpke and H. Schulz, Nucl. Phys. **A477**, 472 (1988).

[15]K. Wildermuth and Y. C. Tang, *A Unified Theory of the Nucleus* (Vieweg, Braunschweig, 1977).

[16]R. J. Griffiths and S. A. Harbison, Ap. J. **158**, 711 (1969); A. M. Sourkes, A. Houdayer, W. T. H. van Oers, R. F. Carlson, and R. E. Brown, Phys. Rev. C **13**, 451 (1976); A. V. Blinov *et al.*, Yad. Fiz. **35**, 523 (1982) [Sov. J. Nucl. Phys. **35**, 301 (1982)].

[17]H. Feldmeier and P. Danielewicz, National Superconducting Cyclotron Laboratory Report MSUCL-833 (1992).

[18]L. D. Landau and E. M. Lifschitz, *Fluid Mechanics* (Pergamon Press, London, 1959).

[19]A. Lang, B. Blättel, W. Cassing, V. Koch, U. Mosel, and K. Weber, Z. Phys. A **340**, 287 (1991).

[20]M. Berenguer, C. Hartnack, G. Peilert, H. Stöcker, W. Greiner, J. Aichelin, and A. Rosenhauer, J. Phys. G **18**, 655 (1992).

[21]H. Stöcker, G. Buchwald, G. Graebner, J. Theis, J. A. Maruhn, and W. Greiner, Nucl. Phys. **A387**, 205c (1982); H. Stöcker and W. Greiner, Phys. Reports **137**, 277 (1986).

[22]H. H. Gutbrod, A. M. Poskanzer, and H. G. Ritter, Rep. Prog. Phys. **52**, 1267 (1989).

[23]V. I. Manko and S. Nagamiya, Nucl. Phys. **A384**, 475 (1982).

[24]H.-A. Gustafsson, H. H. Gutbrod, B. Kolb, H. Löhner, B. Ludewigt, A. M. Poskanzer, T. Renner, H. Riedesel, H. G. Ritter, A. Warwick, and H. Wieman, Phys. Lett. **142B**, 141 (1984).

FIGURE CAPTIONS

Fig. 1. Contour plots of the particle density integrated over the normal to the reaction plane in Au + Au collisions at 250 MeV/nucleon.

Fig. 2. Baryon density along (solid line) and perpendicular (dashed line) to the beam axis at $t = 15.3$ fm/c, in the $b = 0$ Au + Au collision at beam energy of 250 MeV/nucleon.

Fig. 3. Maximum densities reached in the $b = 0$ collisions of heavy nuclei, as a function of the bombarding energy per nucleon. Solid line shows the densities obtained by solving the Rankine-Hugoniot relations for a shock wave.[18]

Fig. 4. Time dependence of different quantities in the $b = 0$ Au + Au reaction at 250 MeV/nucleon. Top panel displays the baryon density at $r = 0$. Squares in the center panel indicate the number of deuterons, and diamonds - the number of $A = 3$ clusters, which survive intact till the end of the reaction. Diamonds, squares, and circles, in the bottom panel, indicate the collective energy per nucleon (3.1) of $A = 3$ clusters, deuterons, and nucleons, respectively.

Fig. 5. Number of protons (circles) and deuterons (squares) emitted per unit spherical angle, as a function of the c.m. polar-angle θ, in the La + La collisions at 246 MeV/nucleon, and in the Au + Au collisions at 250 MeV/nucleon, at different impact parameters.

Fig. 6. Azimuthal distribution about the beam axis at the c.m. longitudinal momentum $p_{||} \simeq 0$, in the semicentral Au + Au collisions at 400 MeV/nucleon. Left panel shows the distribution of all particles, in the third of five multiplicity bins, as determined in the experiment of Ref. 5. Squares and circles in the right panel indicate, respectively, the calculated deuteron and proton distributions, at b = 4 fm.

Fig. 7. Azimuthal distribution about the major axis of the sphericity tensor (3.2), at the momentum component along the axis $p_3' \simeq 0$, in the semicentral Au + Au collisions at 400 MeV/nucleon. Left panel shows the distribution of all particles, in the third of five multiplicity bins, as determined in the experiment of Ref. 5. Squares and circles in the right panel indicate, respectively, the calculated deuteron and proton distributions, at b = 4 fm.

Fig. 8. Mean kinetic energies of protons (circles), deuterons (squares), tritons (triangles), and helions (diamonds) at c.m. polar-angle of 90°, in the Nb + Nb and Au + Au collisions at 250 MeV/nucleon. Left panels display the mean energies determined in the experiment of Ref. 8, as a function of normalized multiplicity. Center and right panels show the results of our calculations as a function of impact parameter in the direct form, and with the final state subjected to a filtering procedure (Ref. 22), respectively. Proton energies in

the Nb + Nb collisions, obtained with the composite production switched off, are indicated by stars.

Fig. 9. Different energies calculated in the Au + Au collisions at 250 MeV/nucleon, as a function of the impact parameter. The top panel shows the final transverse energies averaged over all angles of protons (circles), deuterons (squares), tritons (triangles), and helions (diamonds). Crosses in the top panel indicate twice the mean longitudinal proton energy. The center panel shows collective transverse energy (3.1) of nucleons (circles), deuterons (squares), and A = 3 clusters (diamonds). Stars in the center panel indicate mean transverse energy per nucleon of all particles. Bottom panel shows the longitudinal (filled symbols) and transverse (open symbols) excitation energies at freeze-out, Eq. (3.10), of nucleons (circles), deuterons (squares), and A = 3 clusters (diamonds).

Fig. 10. Spectra of protons (filled circles), deuterons (squares), tritons (triangles), and helions (diamonds) from the b = 0 Au + Au reaction at 250 MeV/nucleon, and from the b = 0 Nb + Nb reaction at 400 MeV/nucleon, in the range of the c.m. polar-angle θ between 60° and 120°. Open circles for the Nb + Nb reaction represent the proton spectrum at 90°, in arbitrary units, measured in Ref. 24 in events with charged-particle multiplicity between 50 and 60. Crossed circles indicate region where proton spectra

were contaminated by misidentified deuterons and tritons.

Fig. 11. Mean out-of-plane $<E_2>$ and in-plane $<E_1'>$ kinetic-energy components of protons (circles), deuterons (squares), tritons (triangles), and helions (diamonds), at $p_3' \simeq 0$. The directions 1′ and 3′ are, respectively, along the minor and major axis of the sphericity tensor (3.2) in the reaction plane, while the direction 2 is out of the reaction plane.

Fig. 12. Differences between mean kinetic energies of composite particles and proton energies at 90° in the $b = 0$ Au + Au collisions, as a function of beam energy. The deuteron-proton differences are represented by squares; triton-proton - by triangles; and helion-proton - by diamonds. The scatter of points reflects statistical errors of the calculations.

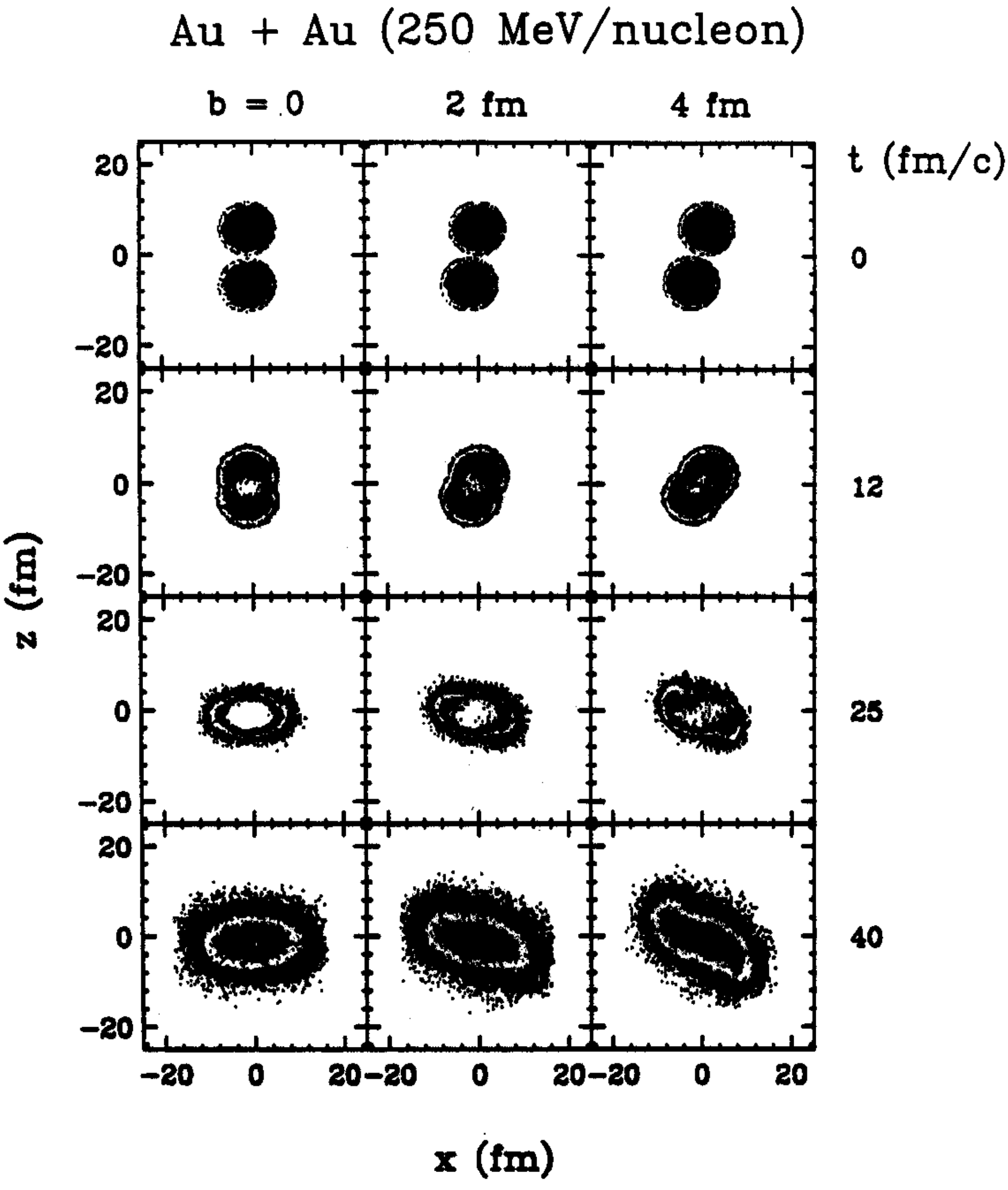

Au + Au (250 MeV/nucleon)
b = 0
2 fm
4 fm
t (fm/c)
0
12
25
40
20
0
−20
z (fm)
−20
0
20
x (fm)

Fig. 1

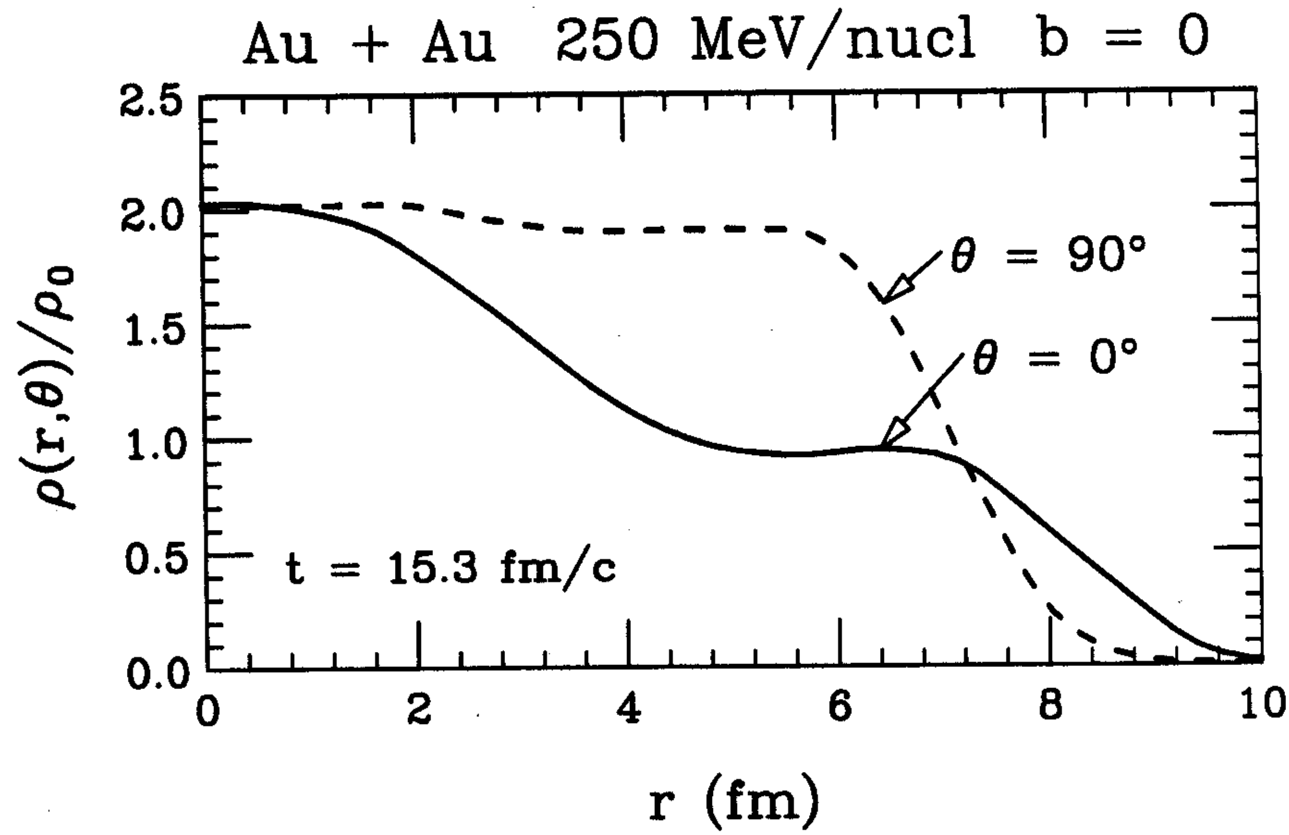

Au + Au 250 MeV/nucl b = 0
$\rho(r,\theta)/\rho_0$
2.5
2.0
1.5
1.0
0.5
0.0
0
2
4
6
8
10
r (fm)
θ = 90°
θ = 0°
t = 15.3 fm/c

Fig. 2

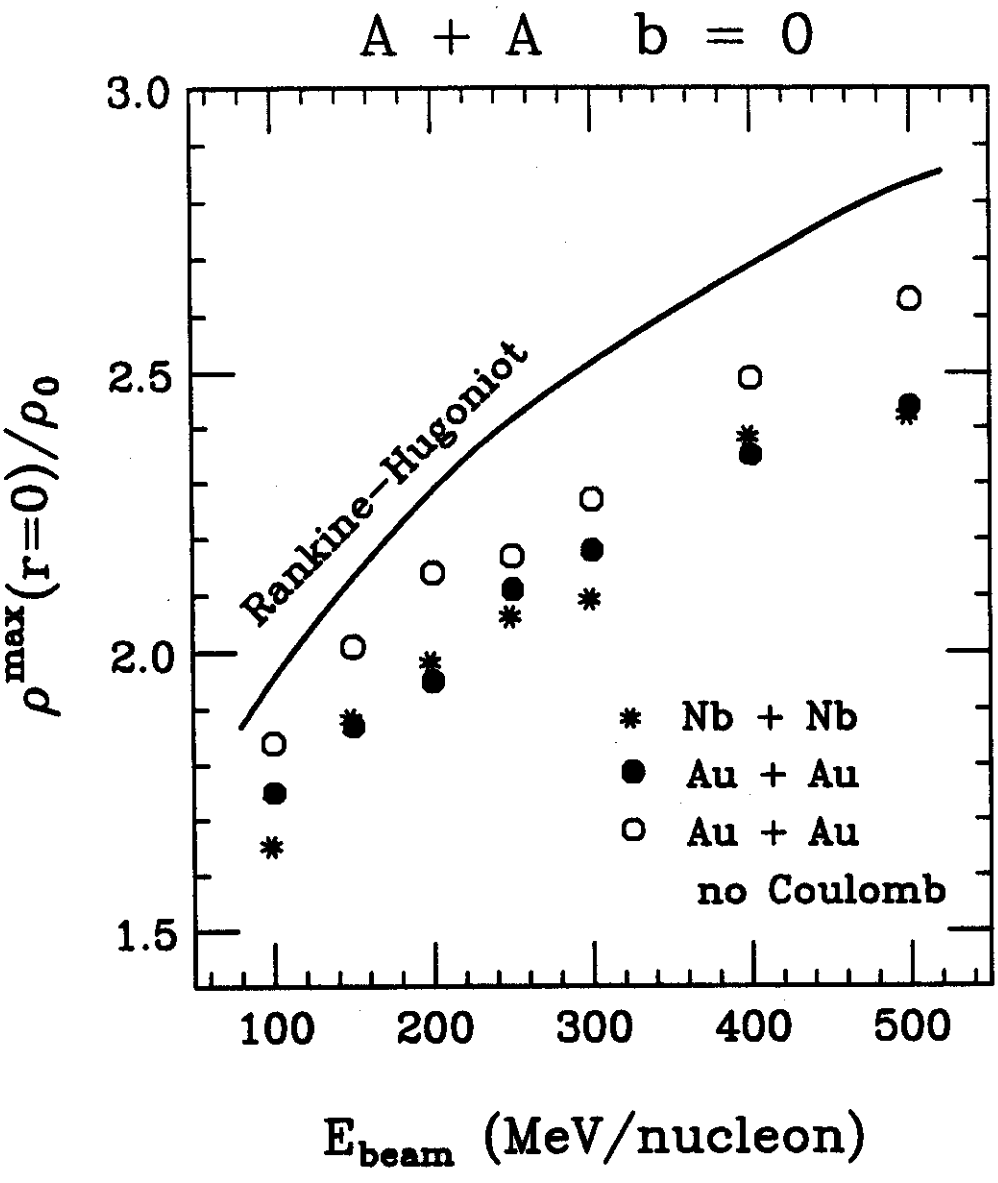
A + A b = 0
3.0
2.5
2.0
1.5
100
200
300
400
500
Rankine–Hugoniot
Nb + Nb
Au + Au
Au + Au
no Coulomb
$\rho^{max}(r=0)/\rho_0$
E_{beam} (MeV/nucleon)

Fig. 3

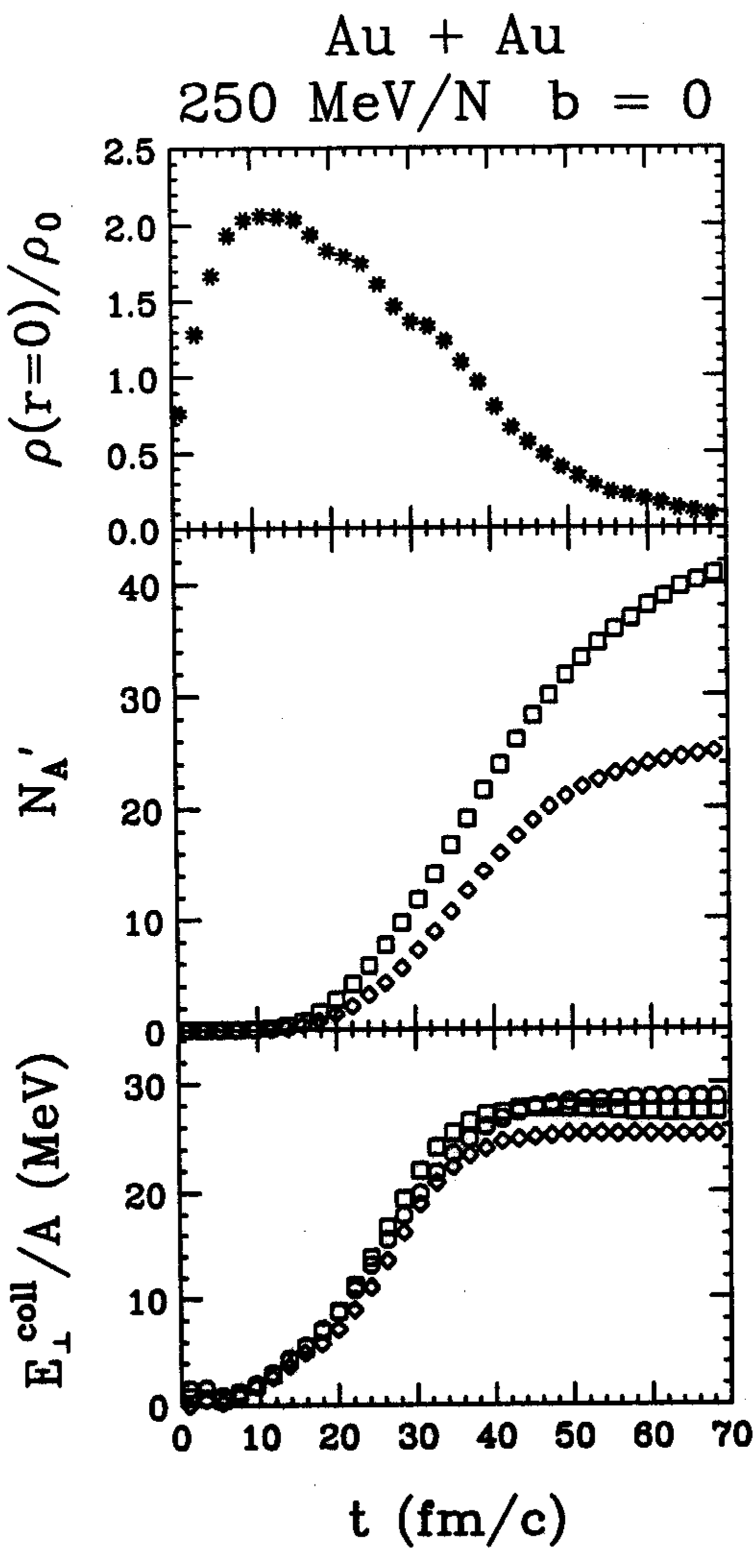

Au + Au
250 MeV/N b = 0
2.5
2.0
1.5
1.0
0.5
0.0
$\rho(r=0)/\rho_0$
40
30
20
10
0
N_A'
30
20
10
0
$E_\perp^{coll}/A$ (MeV)
0 10 20 30 40 50 60 70
t (fm/c)

Fig. 4

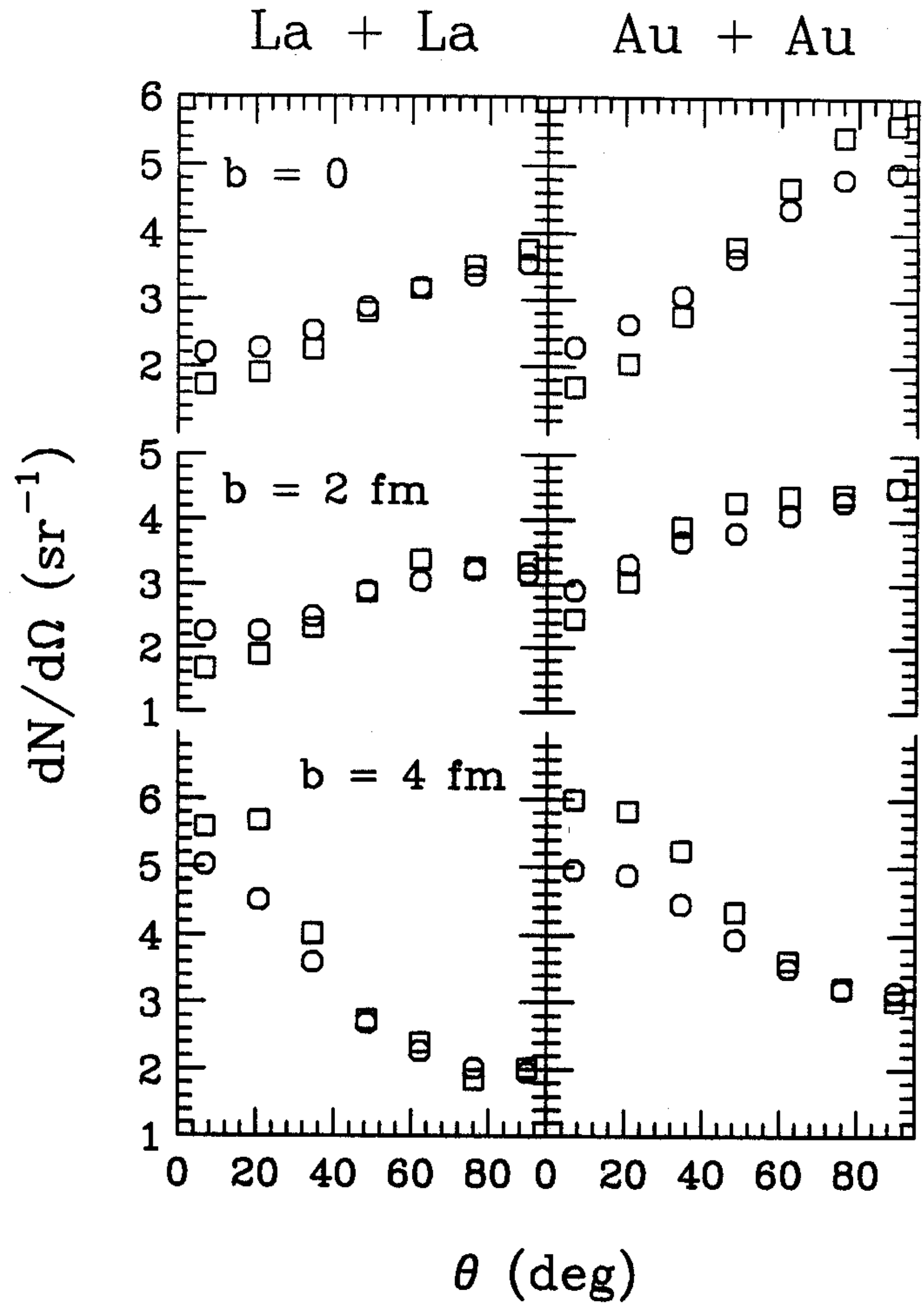

Fig. 5

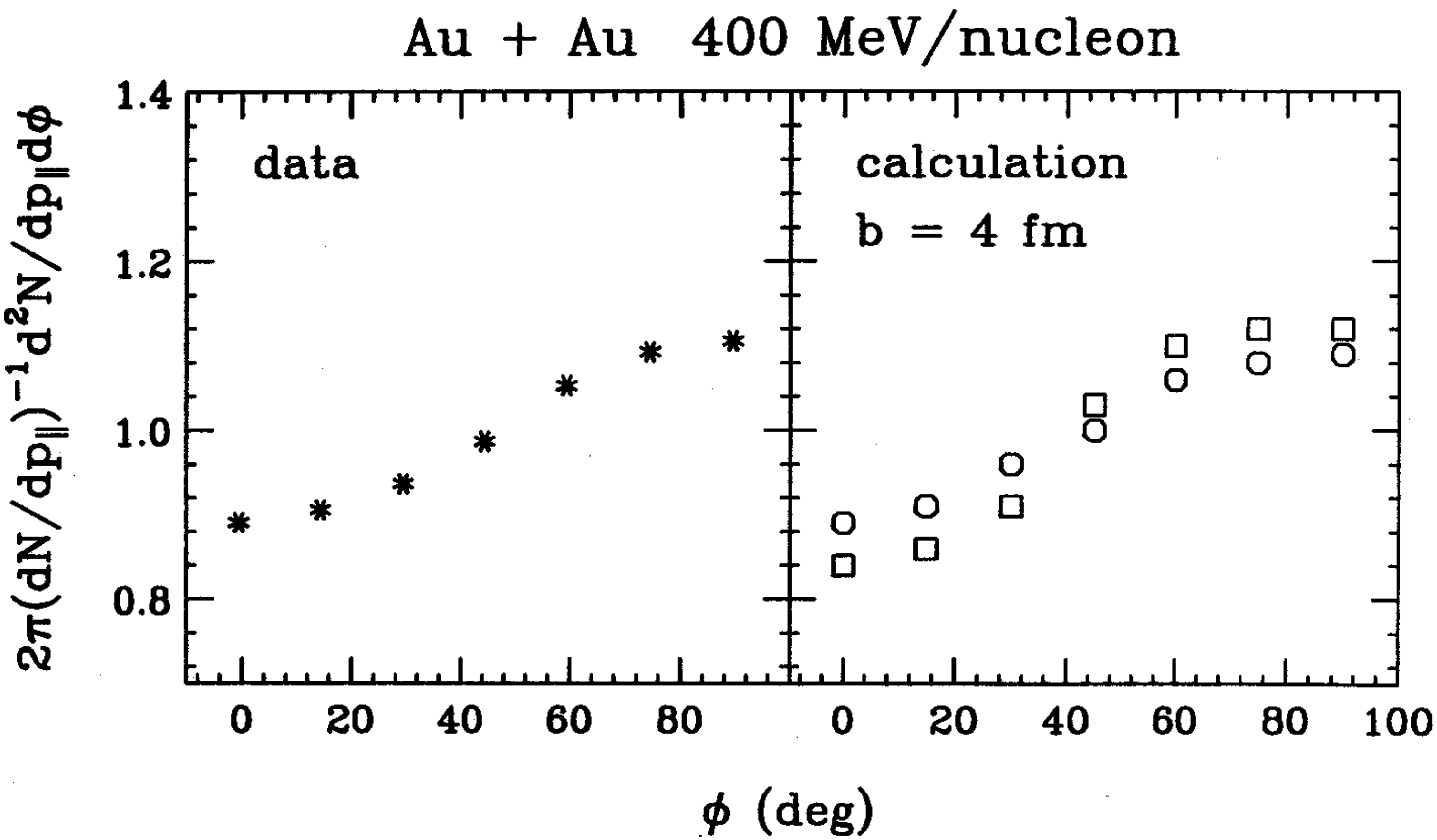

Au + Au 400 MeV/nucleon
data
calculation
b = 4 fm
1.4
1.2
1.0
0.8
0
20
40
60
80
100
$2\pi(dN/dp_\parallel)^{-1}d^2N/dp_\parallel d\phi$
ϕ (deg)

Fig. 6

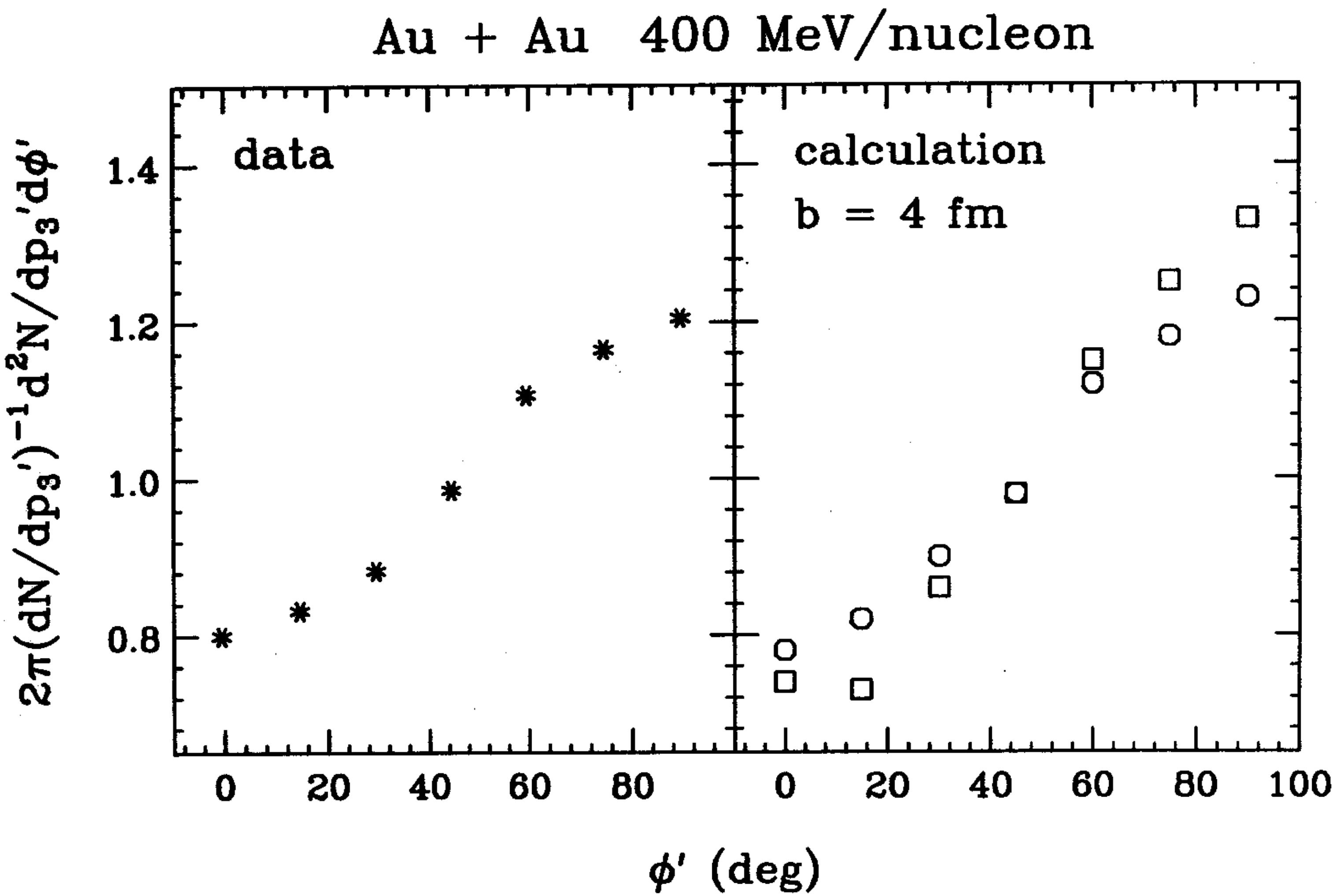

Au + Au 400 MeV/nucleon
data
calculation
b = 4 fm
1.4
1.2
1.0
0.8
$2\pi(dN/dp_3')^{-1}d^2N/dp_3'd\phi'$
0
20
40
60
80
100
ϕ' (deg)

Fig. 7

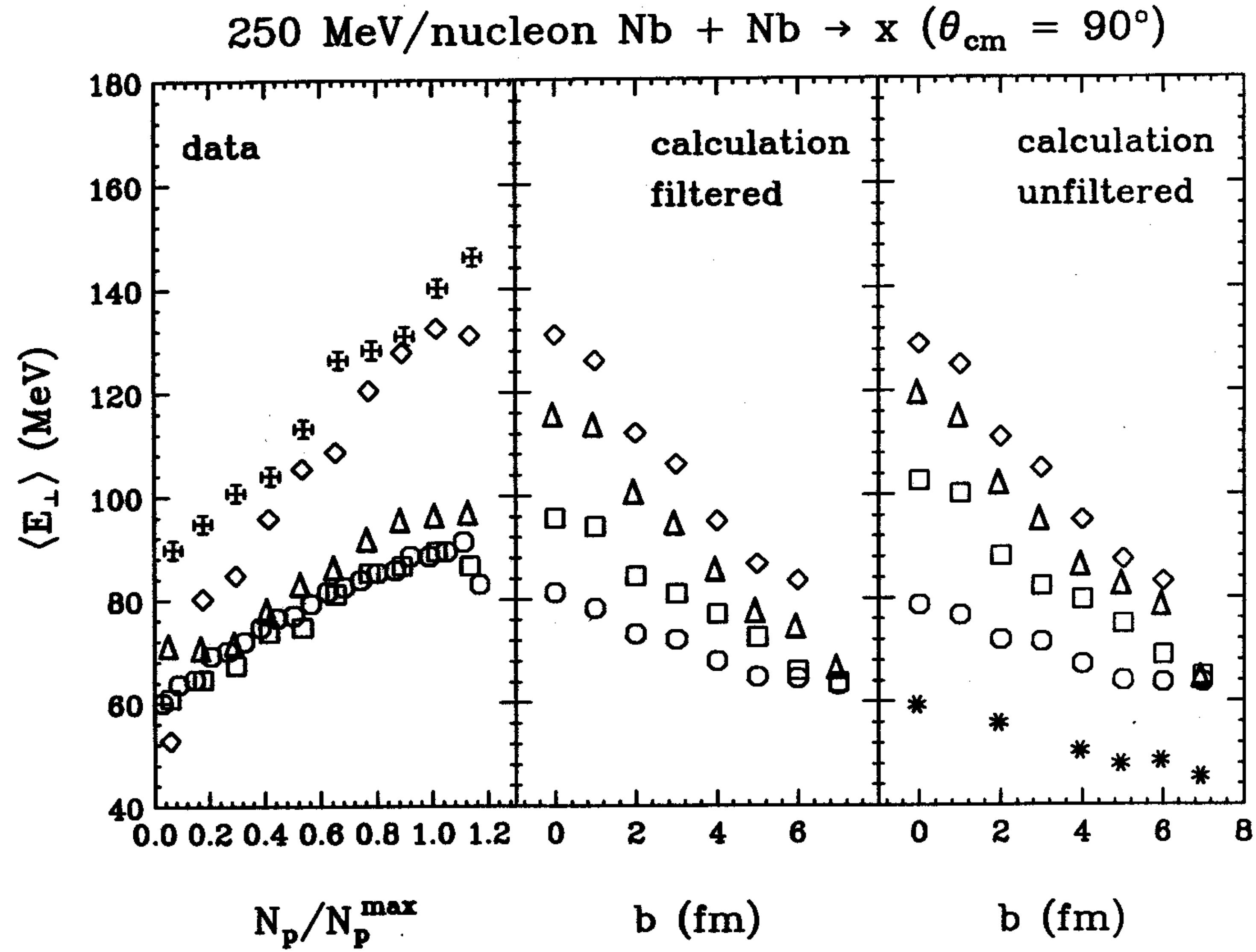

250 MeV/nucleon Nb + Nb → x (θ_{cm} = 90°)
data
calculation filtered
calculation unfiltered
$\langle E_\perp \rangle$ (MeV)
N_p/N_p^{max}
b (fm)
b (fm)

Fig. 8

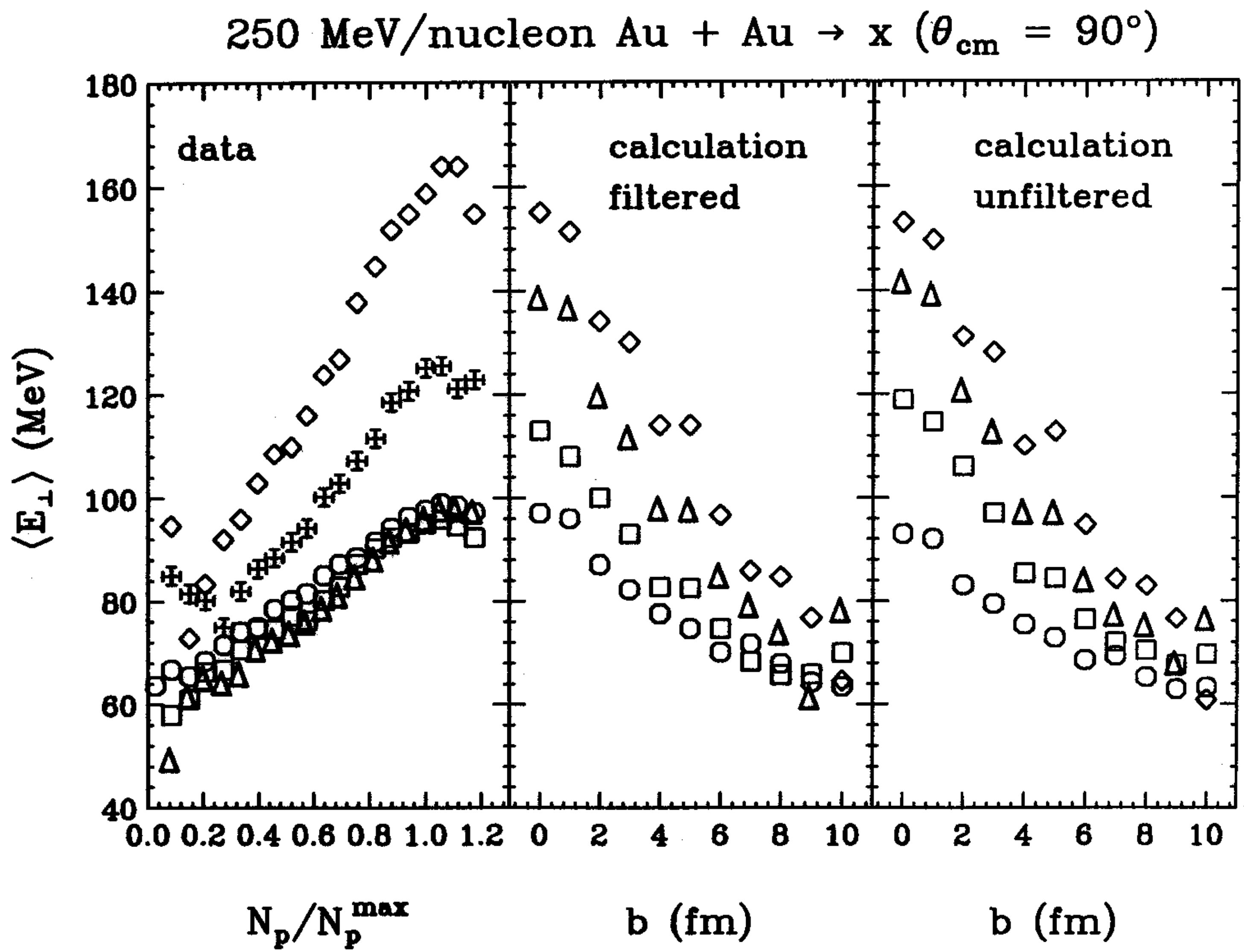

250 MeV/nucleon Au + Au → x (θ_{cm} = 90°)
⟨$E_\perp$⟩ (MeV)
data
calculation
filtered
calculation
unfiltered
N_p/N_p^{max}
b (fm)
b (fm)
180
160
140
120
100
80
60
40
0.0 0.2 0.4 0.6 0.8 1.0 1.2
0 2 4 6 8 10
0 2 4 6 8 10

Fig. 8 cont.

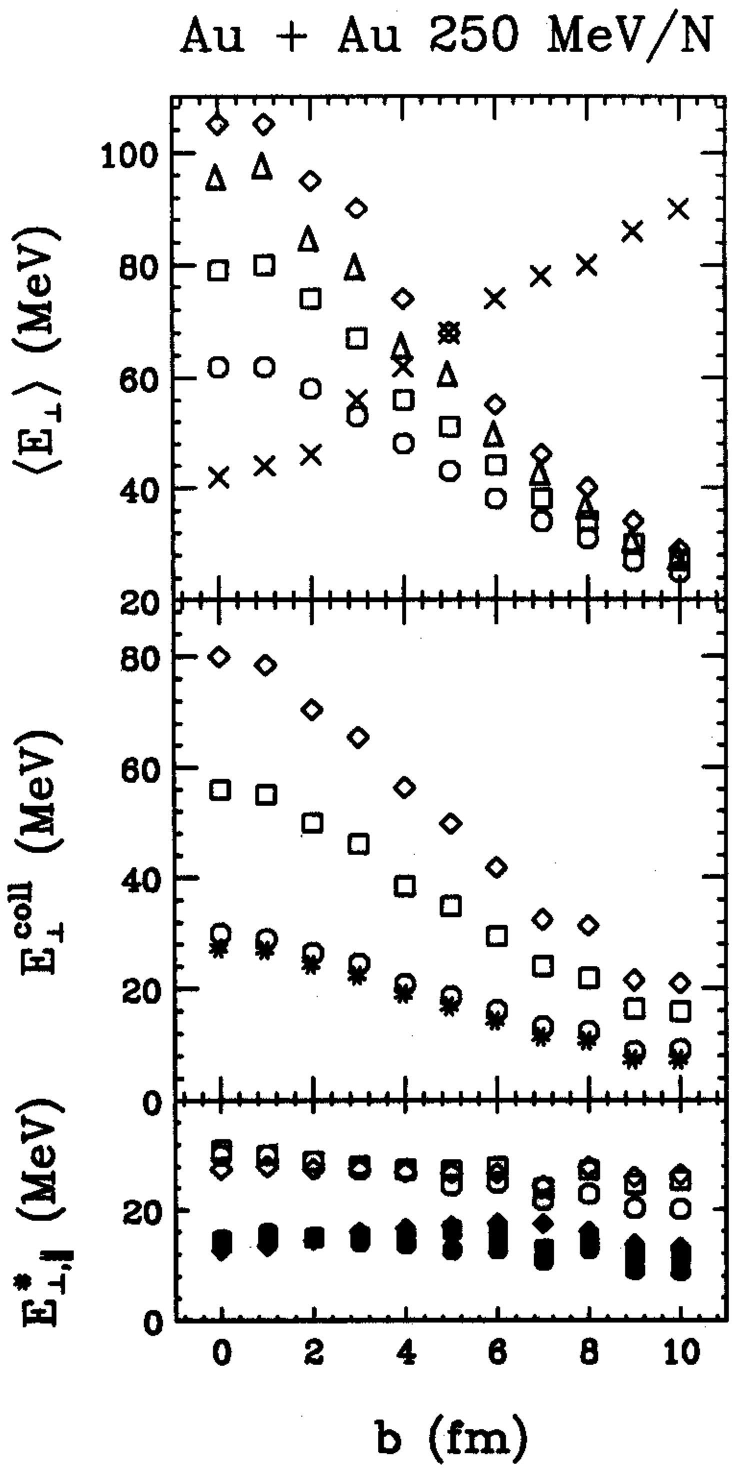
Au + Au 250 MeV/N
$\langle E_\perp \rangle$ (MeV)
$E_\perp^{coll}$ (MeV)
$E^*_{\perp,\parallel}$ (MeV)
b (fm)
100
80
60
40
20
0
2
4
6
8
10

Fig. 9

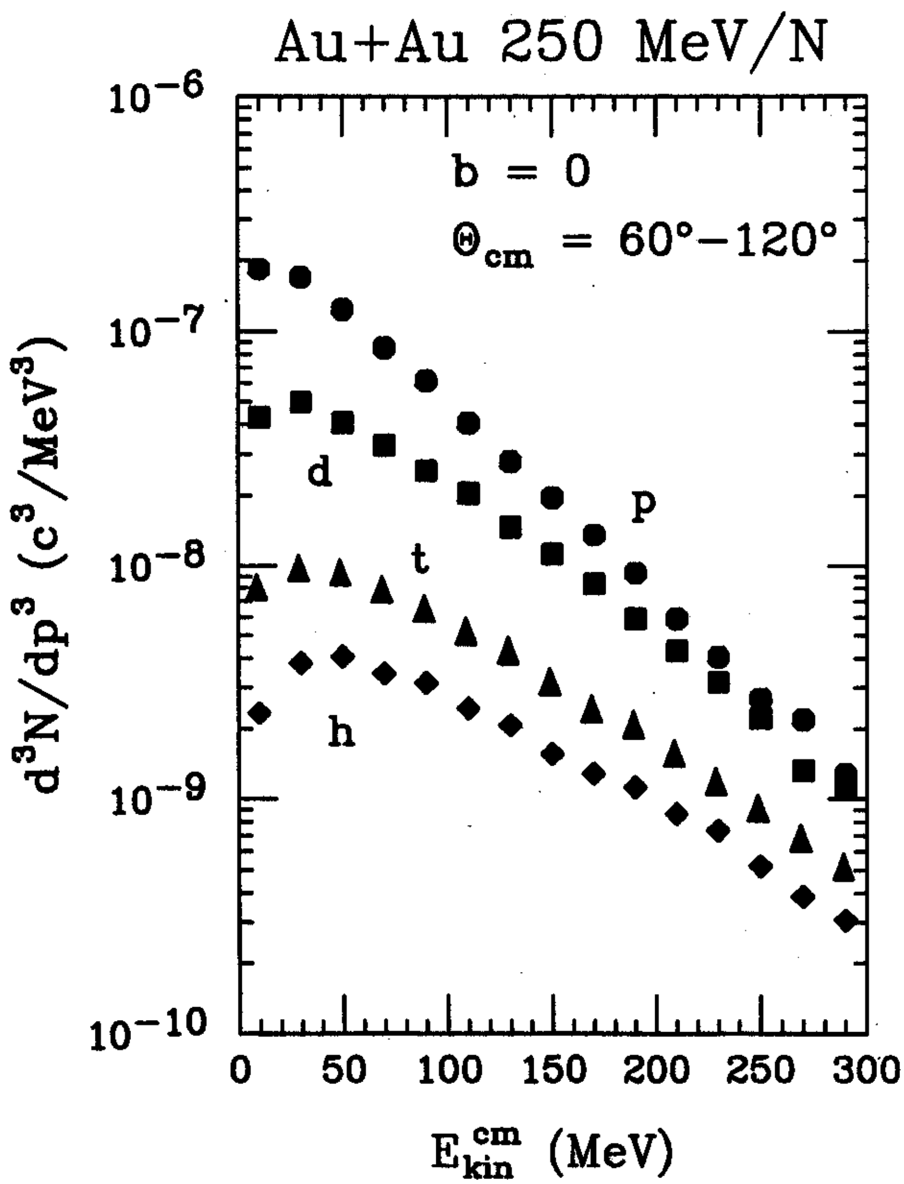

Au+Au 250 MeV/N
b = 0
Θ_{cm} = 60°–120°
p
d
t
h
10^{-6}
10^{-7}
10^{-8}
10^{-9}
10^{-10}
d^3N/dp^3 (c^3/MeV^3)
0
50
100
150
200
250
300
E_{kin}^{cm} (MeV)

Fig. 10

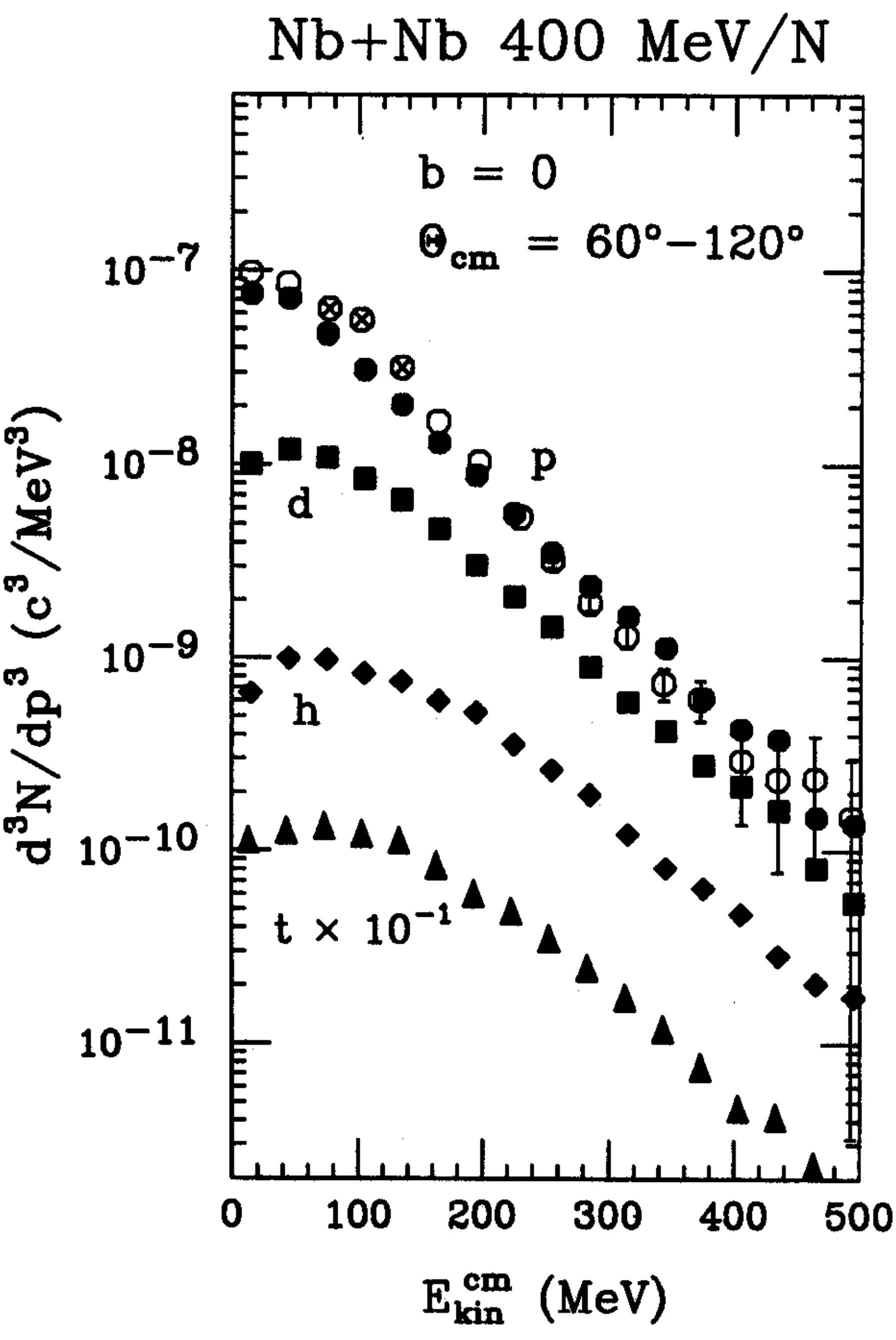
Nb+Nb 400 MeV/N
b = 0
Θ_{cm} = 60°–120°
p
d
h
t × 10^{-1}
d^3N/dp^3 (c^3/MeV^3)
10^{-7}
10^{-8}
10^{-9}
10^{-10}
10^{-11}
0
100
200
300
400
500
E_{kin}^{cm} (MeV)

Fig. 10 cont.

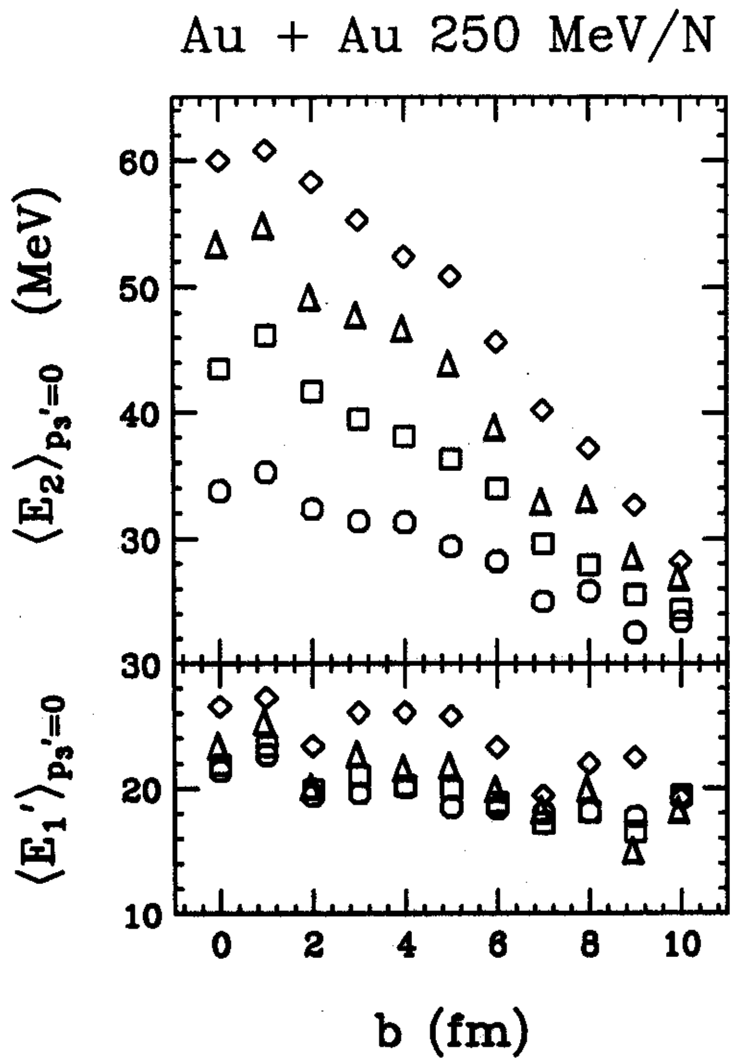
Au + Au 250 MeV/N
$\langle E_2 \rangle_{p_s'=0}$ (MeV)
$\langle E_1' \rangle_{p_s'=0}$
60
50
40
30
30
20
10
0
2
4
6
8
10
b (fm)

Fig. 11

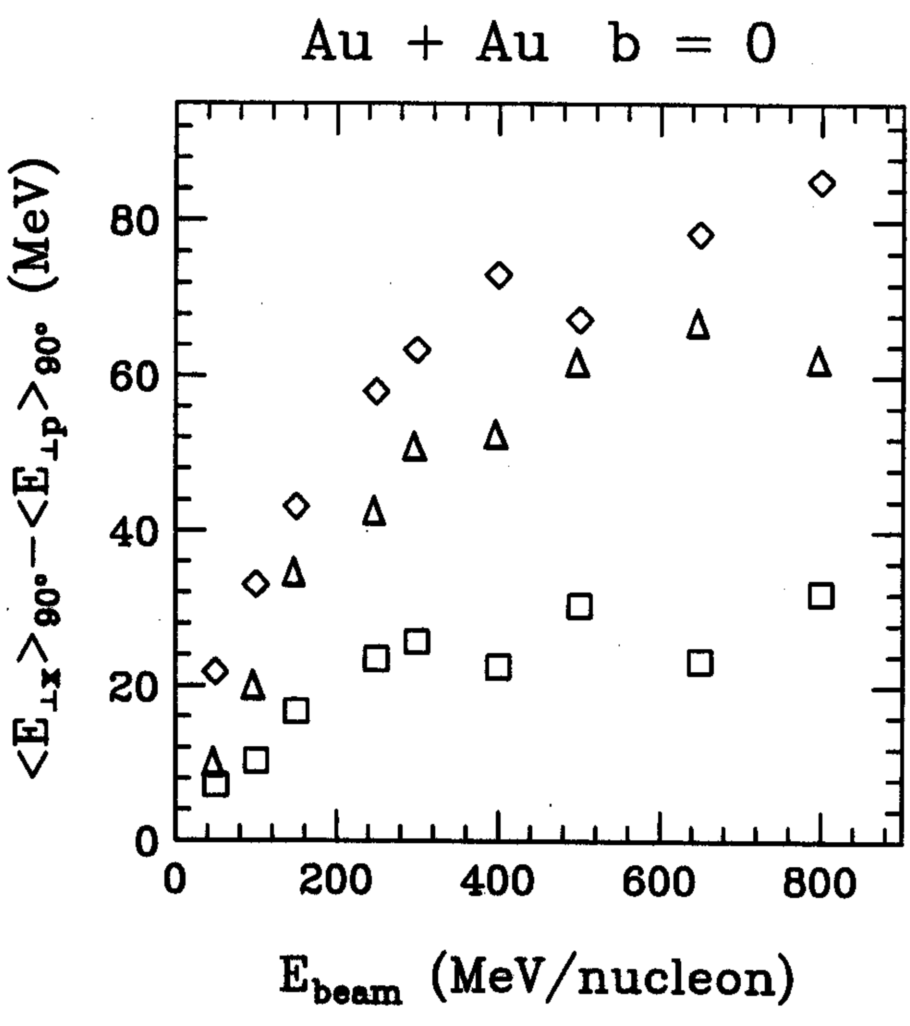

Au + Au b = 0
$\langle E_{\perp x} \rangle_{90^\circ} - \langle E_{\perp p} \rangle_{90^\circ}$ (MeV)
0
20
40
60
80
0
200
400
600
800
E_{beam} (MeV/nucleon)

Fig. 12